Steel and Composite Structures, *Vol. 35, No. 5 (2020) 671-685*
DOI: https://doi.org/10.12989/scs.2020.35.5.671

Static stability and of symmetric and sigmoid functionally graded beam under variable axial load

Ammar Melaibari[1,2], Ahmed B. Khoshaim[1], Salwa A. Mohamed[3] and Mohamed A. Eltaher*[1,4]

[1]Mechanical Engineering Department, Faculty of Engineering, King Abdulaziz University, P.O. Box 80204, Jeddah, Saudi Arabia
[2]Centre of Nanotechnology, King Abdulaziz University, Jeddah, Saudi Arabia
[3]Department of Engineering Mathematics, Faculty of Engineering, Zagazig University,P.O. Box 44519, Zagazig, Egypt
[4]Mechanical Design & Production Department, Faculty of Engineering, Zagazig University,P.O. Box 44519, Zagazig, Egypt

(*Received January 20, 2020, Revised May 13, 2020, Accepted May 23, 2020*)

Abstract. This manuscript presents impacts of gradation of material functions and axial load functions on critical buckling loads and mode shapes of functionally graded (FG) thin and thick beams by using higher order shear deformation theory, for the first time. Volume fractions of metal and ceramic materials are assumed to be distributed through a beam thickness by both sigmoid law and symmetric power functions. Ceramic–metal–ceramic (CMC) and metal–ceramic–metal (MCM) symmetric distributions are proposed relative to mid-plane of the beam structure. The axial compressive load is depicted by constant, linear, and parabolic continuous functions through the axial direction. The equilibrium governing equations are derived by using Hamilton's principles. Numerical differential quadrature method (DQM) is developed to discretize the spatial domain and covert the governing variable coefficients differential equations and boundary conditions to system of algebraic equations. Algebraic equations are formed as a generalized matrix eigenvalue problem, that will be solved to get eigenvalues (buckling loads) and eigenvectors (mode shapes). The proposed model is verified with respectable published work. Numerical results depict influences of gradation function, gradation parameter, axial load function, slenderness ratio and boundary conditions on critical buckling loads and mode-shapes of FG beam structure. It is found that gradation types have different effects on the critical buckling. The proposed model can be effective in analysis and design of structure beam element subject to distributed axial compressive load, such as, spacecraft, nuclear structure, and naval structure.

Keywords: buckling stability; variable axial load; FG sigmoid distribution; higher beam theory; variable-coefficients differential equations; Differential Quadrature Method (DQM)

1. Introduction

Functionally graded materials (FGMs) had been invented in the 1980s by Japanese scientists during the space-plane project, Alshorbagy *et al*. (2011). FGM is an inhomogeneous composite encompassing two/more constituents varied continuously and smoothly along certain direction(s). FGMs are widely used in many scientific and engineering fields, such as aerospace, automobiles, naval structures, nuclear engineering, and biomedical engineering, Eltaher *et al*. (2013a). Applications of FG materials have broadly been spread in nanostructures to achieve light weight, high sensitivity, and desired performance, Eltaher *et al.* (2012).

In 2013, Şimşek and Reddy presented unified higher order beam theory to study buckling of FG microbeam embedded in elastic Pasternak medium. Eltaher *et al*. (2013b, 2014) studied the effect of size-scale on the static stability of FG Euler and Timoshenko nanobeams based on the modified nonlocal continuum model by using finite element method (FEM). Sedighi *et al*. (2015a, b) investigated a dynamic stability of double-sided NEMS fabricated from non-symmetric FGM incorporating finite conductivity, surface energy and nonlocal effect. Eltaher *et al.* (2016) investigated effects of thermal load and shear force on the buckling of higher-order shear deformation nanobeams. Emam and Eltaher (2016) presented effects of temperature variation and moisture absorption on the buckling and post-buckling of composite beams in hydrothermal environments. Khorshidi *et al.* (2016) studied nonlinear post-buckling behavior of FG nanobeams based on modified couple stress theory. Hamed *et al*. (2019) examined effects of porosity models on the static behavior of size dependent FG nanobeam modeled by nonlocal elasticity. Kahya and Turan (2017) developed a finite element model based on shear deformation theory to study vibration and buckling of FG beam. Rahmani *et al.* (2017) derived an analytical solution of buckling of double FG nonlocal nanobeam under axial load. She *et al*. (2017) predicted thermal buckling and post-buckling behaviors of FGM beams based on classical and higher order shear deformation theories. Mohammadimehr *et al.* (2018) studied bending, buckling, and vibration of composite beam reinforced by carbon nanotubes (CNTs) and concluded that 2% of CNTs leads to increase the mechanical properties and increases natural frequencies and critical buckling load, and decreases deflection. Akbas (2018) presented non-linear geometrical effect on the static behavior of FG simple

*Corresponding author, Professor
E-mail: meltaher@kau.edu.sa; mmeltaher@zu.edu.eg

http://www.techno-press.org/?journal=scs&subpage=8 ISSN: 1229-9367 (Print), 1598-6233 (Online)

supported beam including porosity effect. Karami *et al.* (2018) studied thermal buckling of smart porous FG nanobeam rested on Kerr foundation and integrated with piezoelectric sensor and actuator based on the nonlocal higher-order shear deformation beam theory. Mohamed *et al.* (2018) presented a novel numerical procedure to predict nonlinear free vibration and steady state forced vibrations of curved beam in the vicinity of post-buckling configuration. Emam *et al*. (2018) studied postbuckling and free vibration of multilayer imperfect nanobeams under a pre-stress load. Arioui *et al*. (2018) predicted thermal buckling of FG beams having parabolic thickness variation and temperature dependent materials. Eltaher *et al.* (2019) investigated periodic and nonperiodic modes of post-buckling and nonlinear vibration of beams attached to nonlinear foundations. Avcar (2019) studied free vibration of beams made of imperfect FGMs including porosities within the frame works of classical and first order shear beam theories. Abdelrahman *et al*. (2019) and Almitani *et al.* (2019) studied free and forced vibration behaviors of perforated beams by using semi-analytical method. Almitani *et al.* (2020) studied buckling stability of perforated nanobeams incorporating surface energy effects. Mohamed *et al*. (2019 &2020) explored the post-buckling behavior of elastic CNTs modeled by classical and higher shear beam theories using energy equivalent method. Ansari *et al*. (2020) exploited variational differential quadrature finite element method and modifed Halpin-Tsai model to study the vibration and buckling of FG graphene platelets plates with cutout. Kim *et al*. (2020) presented continuum mechanics comprehensive finite element model to analyze multilayered composite beams with interlayer slips. Abdulrazzaq *et al*. (2020) studied thermal buckling of nonlocal clamped exponentially graded plate according to a secant function based on refined theory.

Structure elements such as, rods, beams, plates, and shells are employed frequently as parts in the complex structures. The load exerted on these parts are not always constant or uniform but acting in non-uniform distributions, such as in in aircraft, automotive, civil, and ship-building industries, Eltaher *et al*. (2020). Bert and Devarakonda (2003), state that “The problem of buckling of a rectangular plate subjected to uniformly distributed in-plane compressive loading at each end goes back to 1890”. In 1969 Benoy investigated the buckling of plate under parabolic in-plane compressive loading. Wang *et al*. (1984) presented the buckling of simply supported plate under the linear varying in-plane load. Eisenberger (1991) derived exact solutions for the critical buckling loads of isotropic columns loaded by variable axial load, which described by polynomial expressions.

Kang and Leissa (2005) developed exact solution to study buckling stability of rectangular plates under linearly varying in-plane loading. Duan and Wang (2008) obtained analytical solution in terms of generalized hypergeometric functions for the elastic buckling of heavy column where the weight of the column was treated as a uniformly distributed axial load. Panda and Ramachandra (2010) investigated the effect of non-uniform in-plane loads on buckling stability of rectangular higher order shear deformation plates. Aminbaghai *et al*. (2012) modelled and simulated a free vibration of the 2D FG beams under the effect of large axial force by using FEM. Farajpour *et al*. (2012) presented buckling response of orthotropic single layered graphene sheet under linearly varying in-plane load by using nonlocal continuum mechanics. Mijušković *et al*. (2014) derived exact stress functions to study static stability of isotropic plates under uniaxial and biaxial compression. Lou *et al*. (2016) studied pre-buckling and buckling behaviors of a simply supported FG micro-shell under a combined axial and radial loads by including shear deformable and von Karman’s geometric nonlinearity. Robinson and Adali (2016) computed buckling loads for CNTs under a combination of concentrated and distributed axial loads by using Rayleigh–Ritz method. Murin *et al.* (2016) investigated static, modal and buckling behaviors of FG solid and hollow beam structures with three directional variation of material properties by using FEM. Osmani and Meftah (2018) investigated the lateral buckling of tapered thin walled bi-symmetric beams under combined axial and bending loads with shear deformations effects by using Ritz method. Karamanli and Aydogdu (2019a) studied elastic buckling of isotropic, laminated composite and sandwich beams under numerous axially varying in-plane forces based on a modified shear deformable beam theory. Karamanli and Aydogdu (2019b) illustrated vibration and buckling responses of laminated composite and sandwich microbeams subjected to the linearly variable axial in-plane load. Singh and Harsha (2019) used Navier’s method to investigate the buckling responses of FGM plate subjected to uniform, linear, and non-linear in-plane loads. Aminbaghai *et al*. (2019) presented the influence of the longitudinal variation of the material properties and the secondary torsion moment on the angle of twist and the normal stresses resulting from non-uniform torsion. Ravindran and Bhaskar (2019) presented 3D elasticity solution for unidirectional reinforced composite plates with in-plane uniaxial grading using a series approach. Eltaher *et al.* (2020) studied the static stability of composite beam under variable axial load by using DQM. Eltaher and Mohamed (2020) and Hamed *et al.* (2020a) presented effects of axial load functions and elastic foundations on the static buckling loads and corresponding modes shapes of sandwich composite beam modeled by unified shear deformation theories. Hamed *et al.* (2020b) presented influence of axial load function and optimization on static stability of sandwich FG beams with porous core. Hamed *et al.* (2020c) presented effects of perforation parameters on critical buckling loads and static bending of thin and thick nanobeams for all boundary conditions.

According to literature survey and author’s background, influences of gradation functions (i.e., sigmoid and symmetric) and axial load functions (i.e., constant, linear, and parabolic) on the buckling behavior of FG beam under compressive axial load have not been investigated elsewhere. Thus, the present study fills this gap. The higher order shear deformation is exploited to consider both thin and thick FG beam structure. Because of the load is distributed through axial direction by a function, the obtained equilibrium equation is found to be differential equation with variable coefficients. The differential quadrature method (DQM) is exploited to solve the governing variable coefficients differential equations and convert them to a generalized matrix eigenvalue problem. The current manuscript is structured as follows: - Section 2 will be focused on material gradation functions, constitutive equations, and governing equilibrium equations. Section 3 presents solution strategy and procedure of numerical differential quadrature method (DQM) to solve the governing equilibrium differential equations with variable coefficients. Validation and numerical studies to present influences of gradation functions, material gradation index, load distribution functions, slenderness ratio, and boundary conditions on the buckling loads and related mode-shapes are discussed in detail in section 4. Section 5 highlights and summarizes main remarks and conclusion points in this study.

2. Problem formulation

2.1 Materials gradation

A geometry and loading of functionally graded beam considered through analysis is presented in Fig. (1). A set of Cartesian coordinates (x, z) is proposed to label the material points of the beam in the reference configuration. Here, the material is changed gradually from metal rich pahse at the bottom to the ceramic rich face at the top of the beam through the thickness direction (z), as shown in Fig. (1(a)). The beam with the following dimensions [length (L), thickness (h), and unity width (b)] has subjected to variable axial load N_{axial}, as presented in Fig. (1(b)).

Assuming that, the material constituent varies continuously and smoothly from metal phase (subscript "m") to ceramic phase (subscript "c") according to a power law function. Hence the volume fraction of material constituents can be expressed by

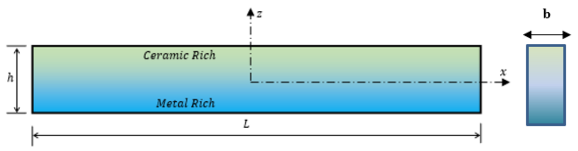

(a) Geometry and Material

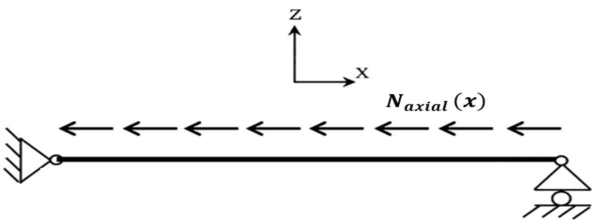

(b) Simply-simply FG beam under axial distributed load $N_{axial}\ (x)$

Fig. 1 Schematic representation of FG beam under distributed axial load $N_{axial}\ (x)$

$$V_c(z) = \left(\frac{h+2z}{2h}\right)^k \quad \& \quad V_m(z) = 1 - V_c(z) \qquad (1)$$

in which $V(z)$ indicates the volume fraction of the constituents and k is the power law index that controls the material constituents. In the current analysis, symmetric power functions and sigmoid function are proposed. In the symmetric power (SP) function, the Young modulus (E) and Poisson's ratio (ν) through the beam thickness can be depicted by, (Hamed *et al.* 2016, Avcar 2019)

SP_ CMC

$$E(z) = E_m + (E_c - E_m)\left(\frac{-2z}{h}\right)^k \qquad \left(-\frac{h}{2} \le z \le 0\right) \quad (2a)$$

$$E(z) = E_m + (E_c - E_m)\left(\frac{2z}{h}\right)^k \qquad \left(0 \le z \le \frac{h}{2}\right) \quad (2b)$$

$$\nu(z) = \nu_m + (\nu_c - \nu_m)\left(\frac{-2z}{h}\right)^k \qquad \left(-\frac{h}{2} \le z \le 0\right) \quad (3a)$$

$$\nu(z) = \nu_m + (\nu_c - \nu_m)\left(\frac{2z}{h}\right)^k \qquad \left(0 \le z \le \frac{h}{2}\right) \quad (3b)$$

SP_MCM

$$E(z) = E_c + (E_m - E_c)\left(\frac{-2z}{h}\right)^k \qquad \left(-\frac{h}{2} \le z \le 0\right) \quad (4a)$$

$$E(z) = E_c + (E_m - E_c)\left(\frac{2z}{h}\right)^k \qquad \left(0 \le z \le \frac{h}{2}\right) \quad (4b)$$

$$\nu(z) = \nu_c + (\nu_m - \nu_c)\left(\frac{-2z}{h}\right)^k \qquad \left(-\frac{h}{2} \le z \le 0\right) \quad (5a)$$

$$\nu(z) = \nu_c + (\nu_m - \nu_c)\left(\frac{2z}{h}\right)^k \qquad \left(0 \le z \le \frac{h}{2}\right) \quad (5b)$$

However, in case of sigmoid functional distribution the Young modulus and Poisson's ratio can be described by, (Hamed *et al.* 2016)

$$E(z) = E_m + \frac{1}{2}(E_c - E_m)\left(1 + \frac{2z}{h}\right)^k \qquad \left(-\frac{h}{2} \le z \le 0\right) \quad (6a)$$

$$E(z) = E_c + \frac{1}{2}(E_m - E_c)\left(1 - \frac{2z}{h}\right)^k \qquad \left(0 \le z \le \frac{h}{2}\right) \quad (6b)$$

$$\nu(z) = \nu_m + \frac{1}{2}(\nu_c - \nu_m)\left(1 + \frac{2z}{h}\right)^k \qquad \left(-\frac{h}{2} \le z \le 0\right) \quad (7a)$$

$$\nu(z) = \nu_c + \frac{1}{2}(\nu_m - \nu_c)\left(1 - \frac{2z}{h}\right)^k \qquad \left(0 \le z \le \frac{h}{2}\right) \quad (7b)$$

The symmetric power and sigmoid FG beams are assumed to be made of aluminum metal [$E_m = 70GPa$, $\rho_m = 2700kg/m^3$ and $\nu_m = 0.3$] and alumina ceramics [$E_c = 380\ GPa$, $\rho_c = 3960\ kg/m^3$ and $\nu_c = 0.3$], Hamed *et al.* (2016). The variation of Young modulus for SP_ CMC , SP_MCM and sigmoid function is shown in Fig. 2.

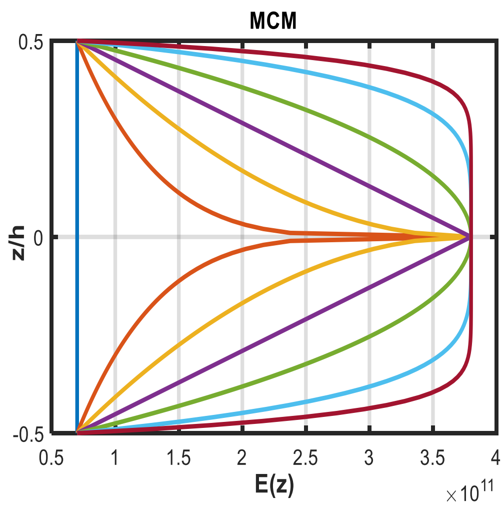

(a) SP-MCM

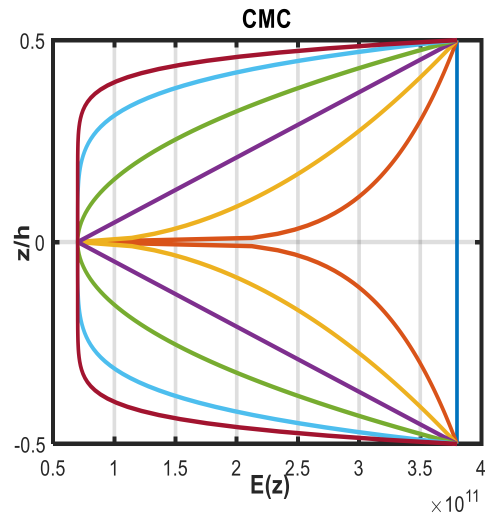

(b) SP-CMC

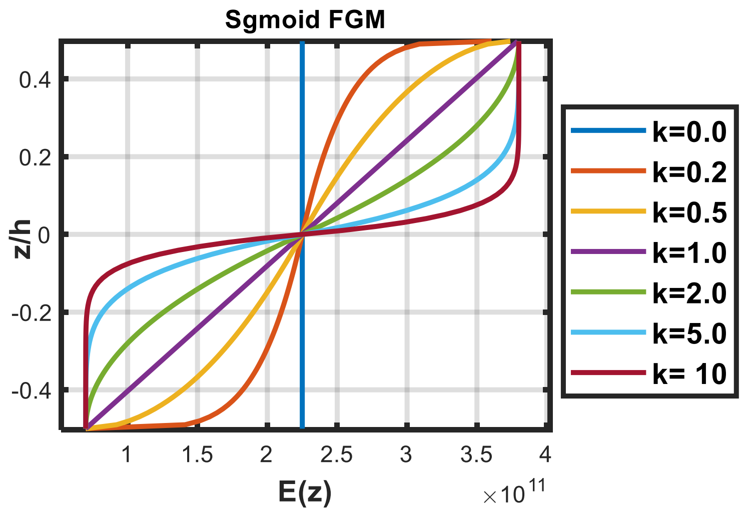

(c) Sigmoid Function

Fig. 2 Variation of Young Modulus through the beam thickness

2.2 Geometrical and constitutive conditions

Based on higher order shear deformation, the enhanced by introducing thickness stretching effects along the transverse directions, Polit *et al.* (2018), kinematic displacement field can be described by Hamed *et al.* (2020)

$$u(x,z) = u_0(x) - z\frac{\partial w_0(x)}{\partial x} + f(z)\varphi(x) \tag{8a}$$

$$w(x,z,t) = w_0(x) \tag{8b}$$

in which u& $w$are a generic axial and transverse displacements through beam domain. However, u_0 and w_0 are the longitudinal and bending displacements of a point along the mid-axis of the beam. The rotation of the normal to the mid-plane is defined by $\varphi(x)$ and $\boldsymbol{f(z)}$ is a function describing the parabolic shear deformation along the thickness and satisfying the zero shear at the top and bottom layers. This function can be portrayed by

$$f(z) = z\left(1 - \frac{4z^2}{3h^2}\right) \tag{9}$$

Strain-displacement field can be derived to

$$\varepsilon_x = \varepsilon_x^0 + zk_x^0 + f(z)k_x^2 \tag{10a}$$

$$\gamma_{xz} = g(z)k_{xz}^s \tag{10b}$$

where $\boldsymbol{\varepsilon_x}$ and $\boldsymbol{\gamma_{xz}}$ are the normal and the shear strains, respectively. The element components of normal and shear strain, described in Eq. (10) can be written as

$$\varepsilon_x^0 = \frac{\partial u_0}{\partial x} \quad , \quad k_x^0 = -\frac{\partial^2 w_0}{\partial x^2} \quad , \quad k_x^2 = \frac{\partial \varphi}{\partial x} \quad , \quad k_{xz}^s = \varphi \quad \& \quad g(z) = \frac{\partial f}{\partial z} \tag{11}$$

The stress-strain constitutive equations can be represented for as, Karamanli and Aydogdu (2019a)

Plane stress components

$$\begin{Bmatrix} \sigma_x \\ \sigma_{zz} \end{Bmatrix} = \begin{bmatrix} Q_{11} & Q_{12} \\ Q_{12} & Q_{22} \end{bmatrix} \begin{Bmatrix} \varepsilon_x \\ \varepsilon_z \end{Bmatrix} \tag{12a}$$

Shear stress component

$$\sigma_{xz} = Q_{55}\ \gamma_{xz} \tag{12b}$$

where the material stiffnesses can be presented in terms of engineering constants as

$$Q_{11}(z) = Q_{22}(z) = \frac{E(z)}{1-\nu^2}, \quad Q_{12}(z) = \frac{\nu E(z)}{1-\nu^2}, \quad Q_{55}(z) = \frac{E(z)}{2(1+\nu)} \tag{13}$$

Based on the higher order shear deformation theory, the force and moment resultants are defined by

Normal force-moment resultants

$$\begin{Bmatrix} N \\ M \\ P \end{Bmatrix} = \begin{bmatrix} A & B & E \\ B & D & F \\ E & F & H \end{bmatrix} \begin{Bmatrix} \varepsilon^0 \\ k^0 \\ k^2 \end{Bmatrix} \tag{14a}$$

Shear force resultant

$$\{R\} = [F^s]\{k^s\} \tag{14b}$$

Axial and bending rigidities (A, B, D, E, F, H), and shear rigidity F^s matrices of FG beam appearing in Eqs. (10) and (11), are evaluated by

$$(A_{ij}\ , B_{ij}\ , D_{ij}) = \int_{-h/2}^{\frac{h}{2}} Q_{ij}[1\ ,\ z,\ z^2]\ dz \quad (i,j = 1,2) \tag{15a}$$

$$(E_{ij}\ , F_{ij}\ , H_{ij}) = \int_{-h/2}^{h/2} Q_{ij}\ f(z)\ [1\ ,\ z,\ f(z)]\ dz \quad (i,j = 1,2) \tag{15b}$$

$$F_{55}^s = \int_{-h/2}^{h/2} g(z) * g(z)\ Q_{55}\ dz \tag{15c}$$

Since the only nonzero force and moment resultant are N_x, M_x , P_x and R_{xz}. So, condensed force, the bending moment, and refined bending moment can be described as functions of strain components, and transformed rigidities as follows, Elather and Mohamed (2020)

$$\begin{Bmatrix} N_x \\ M_x \\ P_x \end{Bmatrix} = \begin{bmatrix} \bar{A}_{11} & \bar{B}_{11} & \bar{E}_{11} \\ \bar{B}_{11} & \bar{D}_{11} & \bar{F}_{11} \\ \bar{E}_{11} & \bar{F}_{11} & \bar{H}_{11} \end{bmatrix} \begin{Bmatrix} \varepsilon_x^0 \\ k_x^0 \\ k_x^2 \end{Bmatrix} \tag{16}$$

in which

$$\begin{bmatrix} \bar{A}_{11} & \bar{B}_{11} & \bar{E}_{11} \\ \bar{B}_{11} & \bar{D}_{11} & \bar{F}_{11} \\ \bar{E}_{11} & \bar{F}_{11} & H_{11} \end{bmatrix} = \begin{bmatrix} A_{11} & B_{11} & E_{11} \\ B_{11} & D_{11} & F_{11} \\ E_{11} & F_{11} & H_{11} \end{bmatrix} - \begin{bmatrix} A_{12} & B_{12} & E_{12} \\ B_{12} & D_{12} & F_{12} \\ E_{12} & F_{12} & H_{12} \end{bmatrix} * \begin{bmatrix} A_{22} & B_{22} & E_{22} \\ B_{22} & D_{22} & F_{22} \\ E_{22} & F_{22} & H_{22} \end{bmatrix}^{-1} \begin{bmatrix} A_{12} & B_{12} & E_{12} \\ B_{12} & D_{12} & F_{12} \\ E_{12} & F_{12} & H_{12} \end{bmatrix} \tag{17}$$

However, the nonzero shear force can be described as function of shear strain and transformed shear rigidities by

$$R_{xz} = (F_{55})k_{xz}^s \tag{18}$$

2.3 Governing equilibrium equations

Based on the Hamilton's principle that states, Eltaher *et al.* (2020)

$$\int_{t_1}^{t_2} (\delta T - \delta V + \delta W)dt = 0 \tag{19}$$

where T, V, and W are the kinetic energy, potential energy, and work done by axial force, respectively. δ denotes the first variation, t_1 and t_2 are arbitrary two instant times. Since, the current article focusing on the static stability of functionally graded composite beam, so that, the kinetic energy can be dropped and $T = 0$. The potential energy for higher order shear theory can be evaluated by

$$V = \frac{b}{2} \int_{-L/2}^{L/2} (N_x\ \varepsilon_x^0 + M_x\ k_x^0 + P_x\ k_x^2 + R_{xz}k_{xz}^s)\, dx \tag{20}$$

By substituting Eqs. (16)-(18) into Eq. (20), the potential energy can be rewritten as

$$\begin{aligned} V = \frac{b}{2} \int_{-L/2}^{L/2} [&(\bar{A}_{11}\varepsilon_x^0 + \bar{B}_{11}k_x^0 + \bar{E}_{11}k_x^2)\ \varepsilon_x^0 \\ &+ (\bar{B}_{11}\varepsilon_x^0 + \bar{D}_{11}k_x^0 + \bar{F}_{11}k_x^2)\ k_x^0 \\ &+ (\bar{E}_{11}\varepsilon_x^0 + \bar{F}_{11}k_x^0 + \bar{H}_{11}k_x^2)\ k_x^2 \\ &+ F_{55}\ k_{xz}^s * k_{xz}^s]\, dx \end{aligned} \tag{21}$$

In the current analysis, it is assumed that the in-plane axial load density (load per unit length) is varied continuously along the beam length by different profiles. It is proposed that, the function depicting the variation of in-plane axial load density can be portrayed by

$$\begin{aligned} N_{axial}\ (x) &= N_{amp}\left[\alpha_2\left(\frac{x}{L}+\frac{1}{2}\right)^2 + \alpha_1\left(\frac{x}{L}+\frac{1}{2}\right) + \alpha_0\right] \\ &= N_{amp}\ C(x) \end{aligned} \tag{22}$$

in which N_{amp} is the average axial load density. According to Eq. (19), the variation profile of axial load distribution can be controlled by the constant coefficients $(\alpha_i), i = 0,1,2$. In this work, the numerical computations are performed for six different axial load distributions as presented in Table 1 and Fig. 3.

It must be mentioned that the coefficients for each of these six types of axially variable load distributions are chosen such that the integral of $N_{axial}\ (x)$ along the beam length are equal. Accordingly, the total axial in-plane force for the considered load types is given by

$$\int_{-L/2}^{L/2} N_{axial}\ (x)\ dx = N_{amp} \int_{-L/2}^{L/2} C(x)dx = N_{amp}L \tag{23}$$

Table 1 Values of the coefficients in Eq. (22) characterizing different types of the axial varying load profile Karamanli and Aydogdu (2019a)

Load Type	Load Symbol	α_2	α_1	α_0
Constant Load	N_{con}	0	0	1
Linear Load-zero from left side	N_{LL}	0	2	0
Linear Load-zero from right side	N_{LR}	0	-2	2
Parabolic Load-zero from left side	N_{PL}	3	0	0
Parabolic Load-zero from right side	N_{PR}	3	-6	3
Symmetric Parabolic Load	N_{PS}	-6	6	0

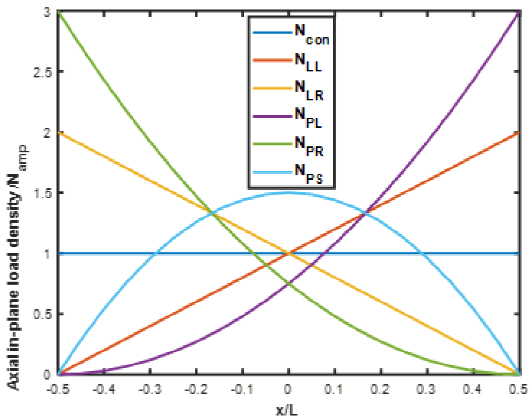

Fig. 3 Axial in-plane load distribution along beam length $C(x) = N_{axial}\ (x)/N_{amp}$

The normalized axial force parameter is defined such that $\lambda = \left(N_{amp}L\right)\frac{L^2}{EI} = N_{amp}\frac{L^3}{EI}$ and similarly, the critical load parameter is $\lambda^{cr} = N_{amp}^{cr}\frac{L^3}{EI}$.

So, the work done by the in-plane axial distributed load is evaluated by

$$W = \frac{b}{2}\int_{-L/2}^{L/2} R(x)\left(\frac{\partial w_0}{\partial x}\right)^2 dx \tag{24}$$

where

$$R(x) = \int_x^{L/2} N_{axial}\ (x)\ dx = N_{amp}L\left[\left(\frac{\alpha_2}{3}+\frac{\alpha_1}{2}+\frac{\alpha_0}{2}\right)-\left(\frac{\alpha_2}{3}\left(\frac{x}{L}+\frac{1}{2}\right)^3+\frac{\alpha_1}{2}\left(\frac{x}{L}+\frac{1}{2}\right)^2+\alpha_0\left(\frac{x}{L}\right)\right)\right] = N_{amp}\hat{R}(x) \tag{25}$$

The variational of the work done can be described as

$$\delta W = b\ \int_{-L/2}^{L/2} R(x)\left(\frac{\partial w_0}{\partial x}\right)\ \left(\frac{\partial\ (\delta w_0)}{\partial x}\right)dx = b\left[R(x)\left(\frac{\partial w_0}{\partial x}\right)\delta w_0\right]_{-L/2}^{L/2} - \int_{-\frac{L}{2}}^{\frac{L}{2}}\frac{\partial}{\partial x}\left(R(x)\frac{\partial w_0}{\partial x}\right)\ \delta w_0\ dx \tag{26}$$

Now, since $\frac{\partial R(x)}{\partial x} = -N_{axial}\ (x)$, so the variation of work done can be represented by

$$\delta W = b\left[R(x)\left(\frac{\partial w_0}{\partial x}\right)\delta w_0\right]_{x=-L/2}^{L/2} - \int_{-L/2}^{L/2}\left(R(x)\frac{\partial^2 w_0}{\partial x^2} - N_{axial}(x)\frac{\partial w_0}{\partial x}\right)\ \delta w_0\ dx \tag{27}$$

By computing the variation of potential energy (V), and substituting the resultant equation and Eq. (24) into variation form of Hamilton principle, the equilibrium equations of higher order shear deformation of FG beam under the in-plane distributed load can be described by

$$\bar{A}_{11}\frac{d^2u_0}{dx^2} - \bar{B}_{11}\frac{d^3w_0}{dx^3} + \bar{E}_{11}\frac{d^2\varphi}{dx^2} = 0 \tag{28a}$$

$$\bar{B}_{11}\ \frac{d^3u_0}{dx^3} - \bar{D}_{11}\frac{d^4w_0}{dx^4} + \bar{F}_{11}\frac{d^3\varphi_0}{dx^3} + N_{amp}\left[\ C(x)\frac{dw_0}{dx} - \hat{R}(x)\frac{d^2w_0}{dx^2}\right] = 0 \tag{28b}$$

$$\bar{F}_{55}\ \varphi - \bar{E}_{11}\frac{d^2u_0}{dx^2} + \bar{F}_{11}\frac{d^3w_0}{dx^3} - \bar{H}_{11}\frac{d^2\varphi}{dx^2} = 0 \tag{28c}$$

subjected to the following boundary conditions

$$\left[\bar{A}_{11}\ \frac{du_0}{dx} - \bar{B}_{11}\frac{d^2w_0}{dx^2} + \bar{E}_{11}\frac{d\varphi}{dx}\right]\delta u_0 = 0 \tag{29a}$$

$$\left[-\bar{B}_{11}\ \frac{d^2u_0}{dx^2} + \bar{D}_{11}\frac{d^3w_0}{dx^3} - \bar{F}_{11}\frac{d^2\varphi}{dx^2} + N_{amp}\ \hat{R}(x)\frac{dw_0}{dx}\right]\delta w_0 = 0 \tag{29b}$$

$$\left[-\bar{E}_{11}\frac{du_0}{dx} + \bar{F}_{11}\frac{d^2w_0}{dx^2} - \bar{H}_{11}\frac{d\varphi}{dx}\right]\delta\varphi = 0 \tag{29c}$$

$$\left[\bar{B}_{11}\ \frac{du_0}{dx} - \bar{D}_{11}\frac{d^2w_0}{dx^2} + \bar{F}_{11}\frac{d\varphi}{dx}\right]\delta w_0' = 0 \tag{29d}$$

3. Solution methodology

The governing equilibrium equations of FG beam under the axial distributed load Eq. (28), and corresponding boundary conditions Eq. (26), are differential equations with variable coefficients. This system of equations requires numerical procedure to be solved. The differential quadrature method (DQM) is proposed to solve this system of equations as following: -

Let the beam length $-\frac{L}{2} \leq x \leq \frac{L}{2}$ be discretized by N nodes using the Chebyshev–Gauss–Lobatto distribution as

$$x_i = -\frac{L}{2} + \frac{L}{2}\left(1 - cos\left(\pi \frac{i-1}{N-1}\right)\right), \qquad i = 1,2,\cdots,N \quad (30)$$

The first order derivative of function $f(x)$ at node x_i can be approximated using the DQM as

$$\left.\frac{df}{dx}\right|_{x=x_i} = \sum_{j=1}^{N} c_{ij} \quad f_j \quad , \qquad i = 1,2,\cdots,N \quad (31)$$

where $f_j = f(x_j)$ and c_{ij} denote the corresponding weighting coefficients. The weighting coefficients can be expressed as follows, Shu (2012)

$$c_{ij} = \frac{1}{x_j - x_i}\left(\frac{P_i}{P_j}\right), \quad i \neq j \qquad and \qquad c_{ii} = -\sum_{j=1, j\neq i}^{N} c_{ij} \quad (32)$$

where

$$P_i = \prod_{j=1, j\neq i}^{N}\left(x_i - x_j\right), \; i,j = 1,2,\cdots,N \quad (33)$$

In matrix form, let the discrete values of $f_i = f(x_i)$ at different nodes be given as a vector $f = [f_1, f_2, \cdots, f_N]^T$. Also, let its first derivative vector be F, then

$$F = \mathcal{C}^{(1)} \; f \quad (34)$$

where $\mathcal{C}^{(1)} = \left[c_{\mathrm{ij}}\right]$ is the weighting $\mathcal{N} \times \mathcal{N}$ matrix of the first order derivative. The weighting coefficients matrices for higher-order derivatives can be determined via matrix multiplication. Matrices $\mathcal{C}^{(1)}, \mathcal{C}^{(2)}, \mathcal{C}^{(3)}$ and $\mathcal{C}^{(4)}$ are coefficients matrices corresponding to the first, second, third and fourth derivatives, respectively. The unknown variables in Eq. (28) are discretized to three unknown vector $U = [u_1, u_2, \dots, u_i, \dots, u_N]^T$, $W = [w_1, w_2, \dots, w_i, \dots, w_N]^T$ and $\varphi = [\varphi_1, \varphi_2, \dots, \varphi_i, \dots, \varphi_N]^T$ where, $u_i = u_0(x_i)$, $w_i = w_0(x_i)$, and $\varphi_i = \varphi_0(x_i)$, $i = 1,2,\cdots,\mathcal{N}$. Also, the given axial load functions $C(x)$ and $\hat{R}(x)$ appearing in Eq. (25(b)) are discretized, respectively, as known vectors $C = [c_1, c_2, \dots, c_i, \dots, c_{\mathcal{N}}]^T$ and $\hat{R} = [r_1, r_2, \dots, r_i, \dots, r_{\mathcal{N}}]^T$.

Accordingly, terms as u_0' , w_0''', φ'' are discretized respectively, by the vectors $\mathcal{C}^{(1)}U, \mathcal{C}^{(3)}W$ and $\mathcal{C}^{(2)}\varphi$. However, to discretize the function $\left(\hat{R}(x)w_0'' - C(x)w_0'\right)$ in Eq. (25(b)), the previously mentioned special matrices multiplications operators are essential. The discrete vector of $\left(\hat{R}(x)w_0'' - C(x)w_0'\right)$ is given by $V = R \circ \left(\mathcal{C}^{(2)}W\right) - C \circ \left(\mathcal{C}^{(1)}W\right)$. Using the operator $\otimes$, this vector can be better written as $V = \left(\hat{R} \otimes \mathcal{C}^{(2)}\right)W - \left(C \otimes \mathcal{C}^{(1)}\right)W$, or as $V = SW$, where matrix S is defined by

$$S = \left(\hat{R} \otimes \mathcal{C}^{(2)}\right) - \left(C \otimes \mathcal{C}^{(1)}\right) \quad (35)$$

The discrete algebraic system corresponding to Eqs. (28) is written as

$$\begin{bmatrix} \bar{A}_{11}\mathcal{C}^{(2)} & -\bar{B}_{11}\mathcal{C}^{(3)} & \bar{E}_{11}\mathcal{C}^{(2)} \\ \bar{B}_{11}\mathcal{C}^{(3)} & -\bar{D}_{11}\mathcal{C}^{(4)} & \bar{F}_{11}\mathcal{C}^{(3)} \\ -\bar{E}_{11}\mathcal{C}^{(2)} & \bar{F}_{11}\mathcal{C}^{(3)} & \bar{F}_{55}I - \bar{H}_{11}\mathcal{C}^{(2)} \end{bmatrix} \begin{bmatrix} U \\ W \\ \varphi \end{bmatrix} = \quad (36)$$

$$N_{amp} \begin{bmatrix} O & O & O \\ O & S & O \\ O & O & O \end{bmatrix} \begin{bmatrix} U \\ W \\ \varphi \end{bmatrix}$$

where I is the identity matrix of order N, and O is the zero matrix of order $N \times N$. The boundary conditions Eq. (29) are discretized and properly substituted into Eq. (36). The resulting system is a generalized eigenvalue problem, that can easily be solved for the eigenvalues (N_{amp}^{cr}), and corresponding eigenvectors or mode-shapes $[U^T, W^T, \varphi^T]^T$. The smallest eigenvalue of the system defines the fundamental buckling load.

4. Numerical results

This section is devoted to three main subsections. The first subsection is focused on validation of proposed model with previous published work. The second one is concerned with physical phenomena and effects of gradation type, gradation index, axial load function, slenderness ratio, and boundary conditions on the critical buckling load of FG thin/thick beams. The last subsection is devoted to the buckling mode-shapes analysis and its effect by loading type. Through current analysis, the critical buckling load parameter λ will be evaluated by

$$\lambda \; = \; N_{amp}^{cr} \frac{L^3}{E_c \; I}$$

in which N_{amp}^{cr} is the critical axial load density obtained as the smallest eigenvalue of Eq. (23).

4.1 Model validation

Since no published results are available in literature for the buckling of SP-FGM or sigmoid-FGM beams under nonuniform distributed axial load, the present approach is validated by considering an isotropic beam subjected to various axially varying distributed loads. In this validation, the present model of CMC- SP-FGM is reduced to represent isotropic beam by setting the gradation index $k = 0$ in Eqs. (2) and (3). The results are presented in Table 2 and compared with those in Eltaher et al. (2020) (*Ref [1]*) and Karamanli and Aydogdu (2019a) *(Ref. [2])* for different boundary conditions (BCs). As depicted, the present results are very closed and excellent agreement to previous works by Eltaher *et al.* (2020) and Karamanli and Aydogdu (2019a) for all boundary conditions and axial load type.

4.2 Parametric analysis

This section is devoted to present impacts of FG distribution, grading index k, boundary conditions, and slenderness ratio on the critical buckling loads for different axial loading types. The symmetric power and sigmoid FG beams are assumed to be made of aluminum metal [$E_m = 70GPa$, $\rho_m = 2700 \; kg/m^3$ and $\nu_m = 0.3$] and ceramics of alumina [$E_c = 380 \; GPa$, $\rho_c = 3960 \; kg/m^3$ and $\nu_c = 0.3$]. Unless mentioned otherwise, the L/h ratio is taken as 20.

Table 2 Critical buckling load parameter $\boldsymbol{\lambda}$ of isotropic beams subjected to various varying axial loads for different BCs. (L/h=100)

		Axial Load Type					
		N_{con}	N_{LL}	N_{LR}	N_{PL}	N_{PR}	N_{PS}
SS	Present	18.5698	15.3529	23.2451	14.1542	26.6870	18.3458
	Ref. [1]	18.564	15.35	23.233	14.152	26.667	18.341
	Ref. [2]	18.5640	15.35	23.2330	14.1520	26.6670	18.3410
CS	Present	52.4704	38.7579	78.9382	34.0914	103.9929	52.2966
	Ref. [1]	52.473	38.749	78.933	34.096	103.973	52.293
	Ref. [2]	52.5759	38.8129	79.1395	34.1485	104.3113	52.5759
CC	Present	74.5419	56.2043	107.6766	50.1905	139.3196	72.6488
	Ref. [1]	74.563	56.219	107.714	50.203	139.382	72.671
	Ref. [2]	74.7772	56.3635	108.0932	50.3271	139.9629	74.7772
CF	Present	7.8487	5.1290	16.0318	4.2280	26.4623	8.7724
	Ref. [1]	7.838	5.122	16.099	4.222	27.252	8.709
	Ref. [2]	7.8548	5.1319	16.1484	4.2292	27.3565	8.7313

where SS (simply-simply BCs), CS (clamped-simply BCs), CC (clamped-clamped BCs), and CF (clamped-free BCs)

4.2.1 Influence of FG distribution types

Influences of gradation function and gradation index on the critical buckling load for different boundary conditions under the parabolic load-zero from right side (N_{PR}) is presented in Fig. 4. As shown, for all boundary condition, the effect of gradation index on the buckling load is dependent mainly on the gradation function type. This means, in case of symmetric power MCM, the critical buckling load is decreased in exponential form as the gradation index increased and reached to steady state at $30 < k$. However, the inverse effect of gradation index on the critical buckling load has been observed in case of symmetric CMC functions distribution. This means, the reduction of critical buckling load by increasing in gradation index. For sigmoid function distribution, the gradation index is insignificant on the critical buckling load for SS boundary condition. However, in cases of other boundary conditions (CC, CS, CF) for sigmoid function distribution, the critical buckling load is decreased significantly by increasing gradation index.

Quantitative effects of gradation function and gradation index on the critical buckling load for SS and CC FG beam structure under the parabolic axial load-zero from right side (N_{PR}) is illustrated in Table 3. For SS boundary condition, by increasing the gradation index from 0 to 0.2, the critical buckling load decreases by 5.2% and 0.4% for CMC and sigmoid functions, respectively. However, the buckling load increases by 28.2% as the gradation index from 0 to 0.2 for MCM gradation type. In case of CC boundary condition, the critical buckling load is decreased by 5.7% and 2% for CMC and sigmoid functions, respectively, by changing gradation index from 0 to 0.2. As the gradation index increased from 0 to 100, CMC decreases by 78% for SS and CC boundary conditions, sigmoid function decreases by 11% and 35% for SS and CC boundary conditions respectively, and MCM increases by 430% for SS and CC boundary conditions.

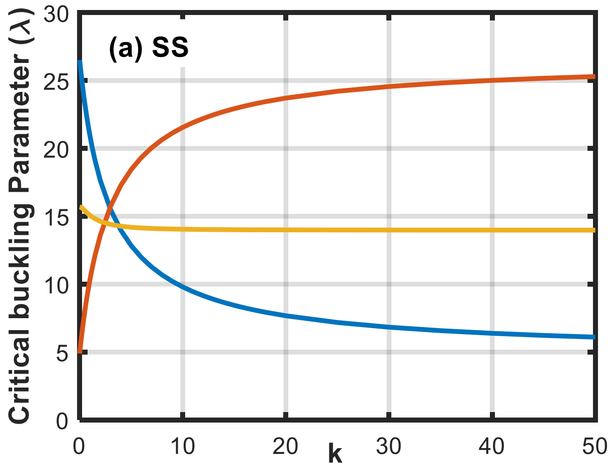

(a)

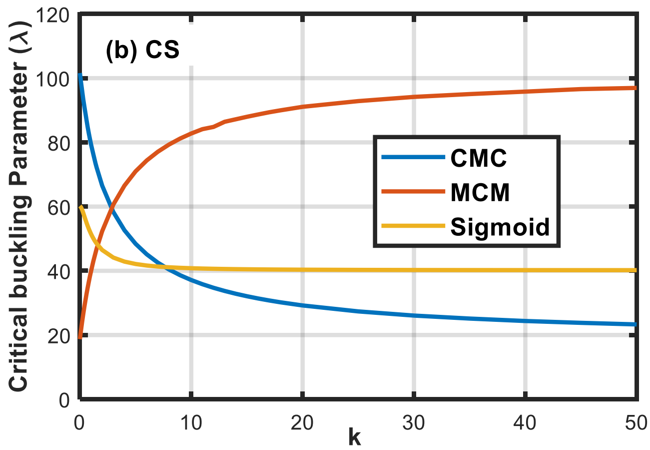

(b)

Continued-

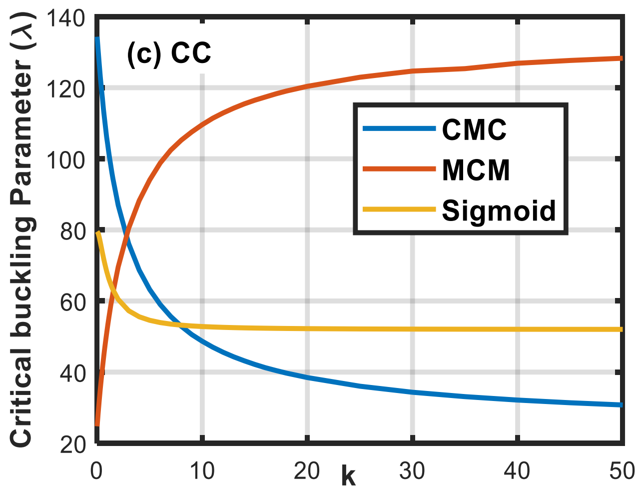

(c)

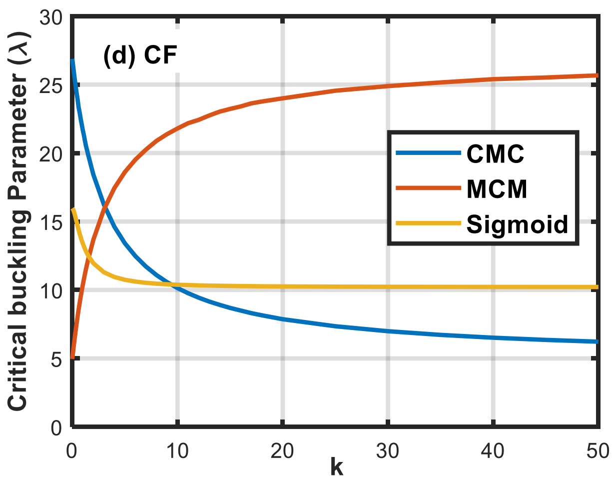

(d)

Fig 4 Influence of gradation index $\boldsymbol{k}$ on dimensionless critical buckling load of beams under N_{PR} varying axial loading with different FGM types for (a) SS, (b) SC, (c) CC and (d) CF

It is noticed that at $k = 0$, the higher buckling load is observed for CMC gradation function and lower buckling load is noticed for MCM gradation type. For higher value of gradation index at $5 < k$, the higher buckling load is observed for MCM gradation function and lower buckling load is noticed for CMC gradation type.

The effect of boundary conditions on the buckling mode shapes of FG beam under N_{PR} is presented in Fig 5. It is noticed that the first mode shape for SS and CC is asymmetric, even though the boundary conditions are symmetric. This due to the distribution of the N_{PR} load is asymmetric. The current mode shapes can be applicable for any gradation index or gradation function because the variation of material constitution occurs in the thickness direction and not in the axial direction. In other words, the mode shapes are independent neither on type nor index value of the FGM distribution.

Table 3 Critical buckling load parameter $\lambda = N_{axil}^{cr} \times 12E_cL^3/h^3$ for SS and CC FG beams under N_{PR}

$k \downarrow$	SS		
	CMC	MCM	Sigmoid
0	26.509	4.883	15.696
0.2	25.108	6.259	15.622
0.5	23.311	8.009	15.409
1	20.929	10.335	15.068
2	17.640	13.585	14.628
5	12.832	18.445	14.189
100	5.508	25.884	13.976
$k \downarrow$	CC		
	CMC	MCM	Sigmoid
0	134.344	24.748	79.540
0.2	126.637	32.035	77.935
0.5	117.084	41.078	73.578
1	104.060	53.030	67.357
2	86.929	69.584	60.458
5	63.220	94.063	54.563
100	27.846	131.250	51.989

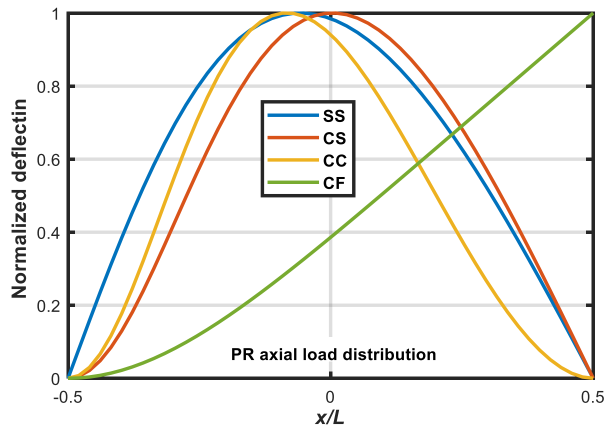

Fig. 5 Buckling mode shapes of FG beams under N_{PR} axial load for different boundary conditions

4.2.2 Influence of axial load type

The impact of axial load type and gradation index on the critical buckling load for SS boundary condition beam at different gradation functions is presented in Fig. 6. As illustrated in Figs. 6(a) and 6(c) for CMC and sigmoid gradation types, the buckling load is decrease significantly by increasing the gradation index. For MCM gradation type as shown in Fig. 6(b), the critical buckling load is increased by increasing the gradation index. The lowest buckling load is observed in case of loading type of N_{PL} , and the highest buckling load is noted in case of N_{PR} for all gradation types. It is also noted that the critical buckling loads for loading conditions N_{con} and N_{Ps} are very close to each

Table 4 Critical buckling load parameter $\boldsymbol{\lambda}$ for SS FG beams under different axial varying load types and different FG distribution types

	$FG\_type \downarrow$	$k \downarrow$	N_{con}	N_{LL}	N_{LR}	N_{PL}	N_{PR}	N_{PS}
SS	CMC	0	18.441	15.245	23.084	14.055	26.509	18.212
		1	14.581	12.059	18.237	11.119	20.929	14.397
		10	6.822	5.642	8.532	5.202	9.792	6.736
	MCM	0	3.397	2.808	4.252	2.589	4.883	3.355
		1	7.185	5.939	8.998	5.475	10.335	7.097
		10	14.988	12.390	18.765	11.422	21.551	14.802
	Sigmoid	0	10.919	9.027	13.668	8.322	15.696	10.783
		1	10.458	8.631	13.105	7.955	15.068	10.312
		10	9.706	7.988	12.189	7.357	14.046	9.548

other. Generally, the critical buckling load is highly dependent on the axial varying load type and its values decreases in the order: N_{PR} ,N_{LR} , N_{con} ,N_{Ps} , N_{LL}, and then N_{PL} . A quantitative analysis of Fig. 6 is presented in Tables 4 and 5 for SS and CC FG beams.

4.2.3 Influence of aspect ratio

The effects of slenderness ratio on FG beam subjected to parabolic distribution axial load from right N_{PR} for different gradation index, gradation function, boundary conditions

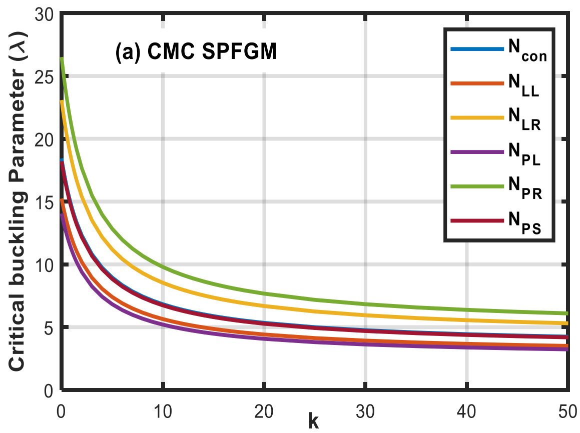

(a)

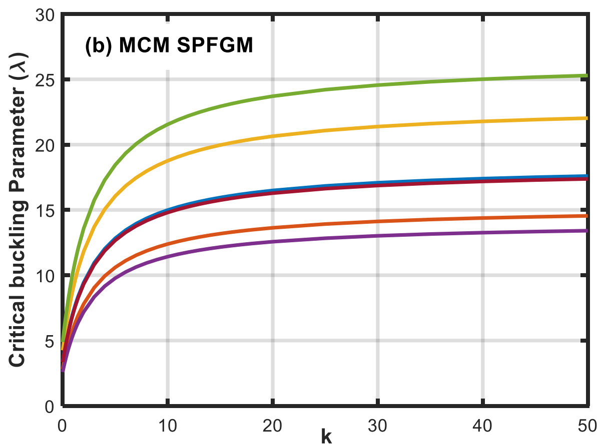

(b)

Continued-

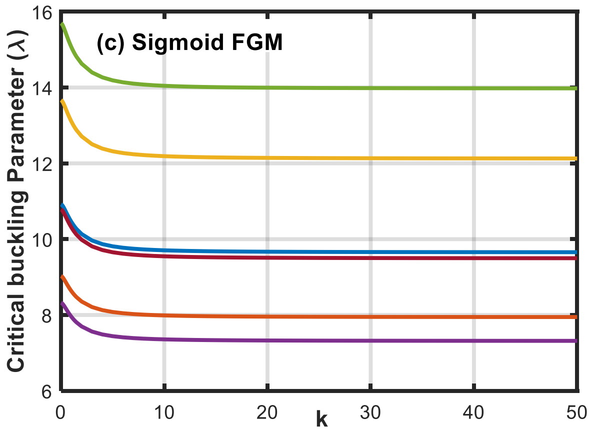

(c)

Fig. 6 Influences of the gradation index k on the critical buckling load parameter λ of a SS beam under different axial varying load types and different FG distribution types (a) CMC-SPFGM, (b) MCM-SPFGM and (c) sigmoid-FGM

are presented in Table 6. As shown the buckling load is decreased significantly by increasing the slenderness ration from 10 to 20 for the same conditions, due to the contribution of the shearing effect. However, increasing slenderness ration more than the 20, the FG beam becomes thin and effect of shearing is reduced and hence, the slenderness ratio has not significant influence on buckling loads. Qualitative analysis of Table 6 is presented in Fig. 7, to illustrate the significance region of slenderness ratio on the critical buckling load for FG beam with different gradation index, gradation function, and boundary conditions. The same observation deduced from Table 6 is noted in Fig. 7.

Table 5 Critical buckling load parameter $\boldsymbol{\lambda}$ for CC FG beams under different axial varying load types and different FG distribution types

	FG_type ↓	k ↓	N_{con}	N_{LL}	N_{LR}	N_{PL}	N_{PR}	N_{PS}
CC	CMC	0	72.647	54.755	104.296	48.923	134.344	70.594
		1	56.553	42.753	81.058	38.205	104.060	54.988
		10	26.454	19.993	37.907	17.872	48.668	25.729
	MCM	0	13.359	10.082	19.213	9.013	24.748	13.003
		1	28.518	21.503	41.064	19.209	53.030	27.753
		10	59.109	44.617	85.058	39.863	109.609	57.535
	Sigmoid	0	42.939	32.422	61.736	28.980	79.540	41.793
		1	36.317	27.409	52.256	24.488	67.357	35.348
		10	28.415	21.443	40.933	19.155	52.815	27.669

Table 6 Critical buckling load parameter for beams under $\boldsymbol{N_{PR}}$ axial load and different FGM types, gradation index and boundary conditions

		CMC			MCM			Sigmoid		
	L/h ↓ k →	0	1	100	0	1	100	0	1	100
SS	10	25.631	19.7677	5.312	4.721	10.143	25.038	15.176	14.596	13.600
	20	26.509	20.9290	5.507	4.883	10.335	25.883	15.696	15.067	13.975
	30	26.654	21.1536	5.541	4.910	10.359	26.023	15.782	15.142	14.027
	50	26.696	21.2433	5.552	4.917	10.361	26.062	15.807	15.160	14.034
	100	26.687	21.2486	5.550	4.916	10.357	26.052	15.801	15.152	14.026
CS	10	94.151	70.1282	19.401	17.342	38.235	92.124	55.707	48.184	38.466
	20	101.592	79.3527	21.079	18.716	39.865	99.299	60.183	51.476	40.168
	30	103.021	81.3343	21.404	18.977	40.172	100.585	60.986	52.094	40.312
	50	103.714	82.3396	21.562	19.105	40.317	101.258	61.409	52.388	40.242
	100	103.992	82.7222	21.622	19.153	40.372	101.507	61.565	52.492	40.143
CC	10	120.487	145.938	24.750	22.201	49.544	116.895	71.031	61.362	48.547
	20	134.343	104.059	27.846	24.748	53.030	131.250	79.539	67.356	51.988
	30	137.180	107.868	28.486	25.269	53.637	133.956	81.226	68.560	52.669
	50	138.675	109.927	28.823	25.545	53.971	135.394	82.111	69.189	53.022
	100	139.319	110.764	28.970	25.664	54.111	136.017	82.492	69.460	53.174
CF	10	28.974	24.9175	5.951	5.238	10.666	27.074	16.917	13.877	10.468
	20	26.882	21.6653	5.604	4.958	10.375	26.263	15.963	13.394	10.210
	30	26.666	21.3469	5.549	4.911	10.310	26.027	15.790	13.274	10.140
	50	26.524	21.1636	5.518	4.886	10.281	25.892	15.704	13.214	10.105
	100	26.462	21.077	5.503	4.8746	10.267	25.833	15.668	13.188	10.090

4.3 Buckling mode-shape

Impacts of the proposed loading types on the first buckling mode-shapes on different boundary conditions are illustrated in Fig. 8. It is observed that for beams with symmetric boundary conditions (SS, CC) even in case of constant density axial load distribution, the buckling mode shapes are asymmetric due to the accumulated nature of the axial load. It is also observed that for all boundary conditions, the mode shapes are dependent on the axial varying load type and they are shifted to left in the order: N_{PR} , N_{LR} , N_{con} , N_{Ps} , N_{LL} , and then N_{PL} .

Fig. 9 presents the effect of parabolic distrbution of axial compressive load on the first buckling mode of FG beam under different boundary conditions. As shown for all boundary conditions, with respect to the buckling mode shapes of N_{Ps} , the mode shapes of N_{PR} and N_{PL} are shifted to left and right, respectively.

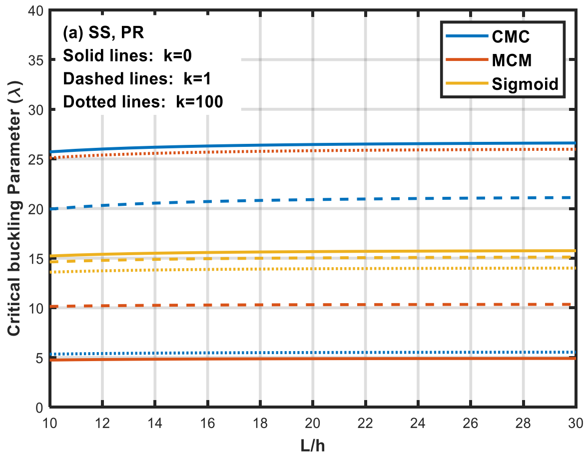

(a)
Continued-

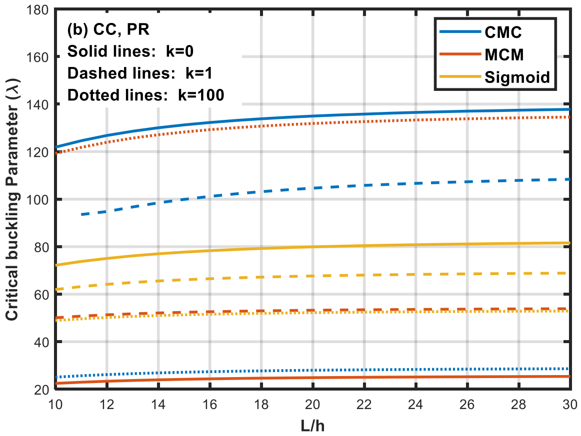

(b)

Fig. 7 Influence of aspect ratio L/h on critical buckling load parameter of (a) SS and (b) CC beams under N_{PR} varying axial load for different FGM types and gradation index

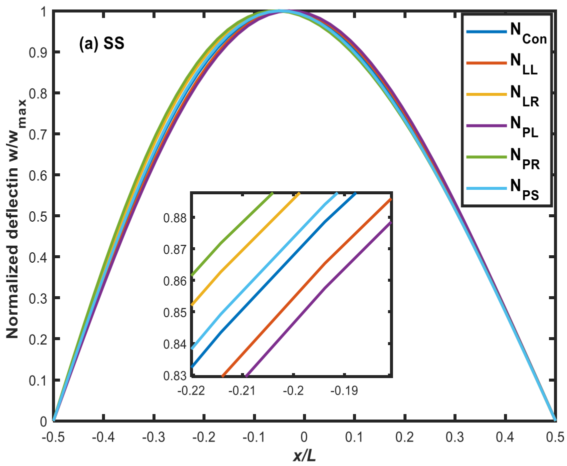

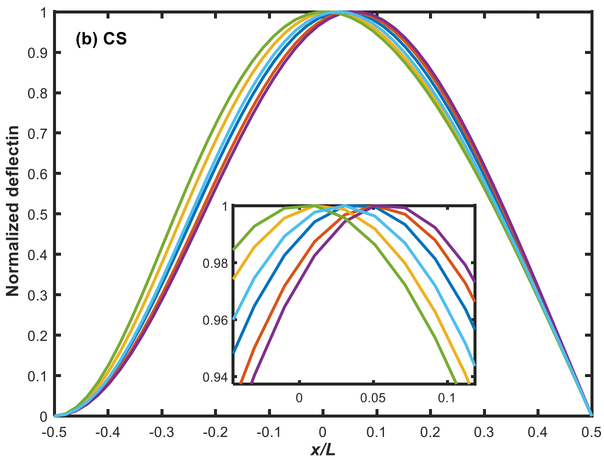

Continued-

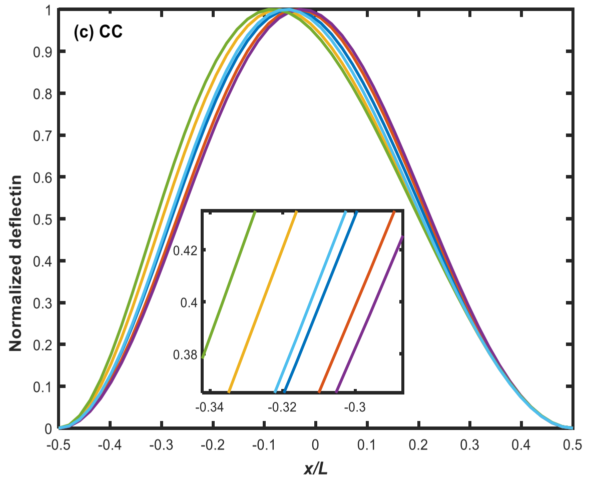

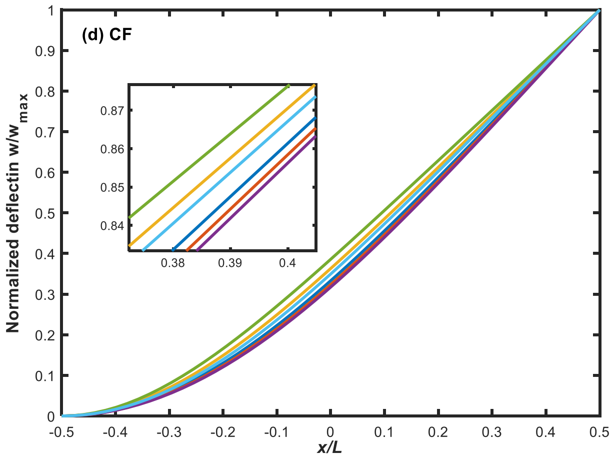

Fig. 8 Influence of axial load distributions on buckling mode shapes of FGM beams for different boundary conditions

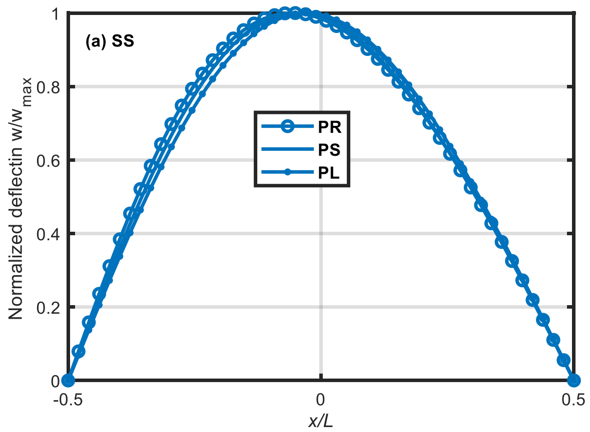

Continued-

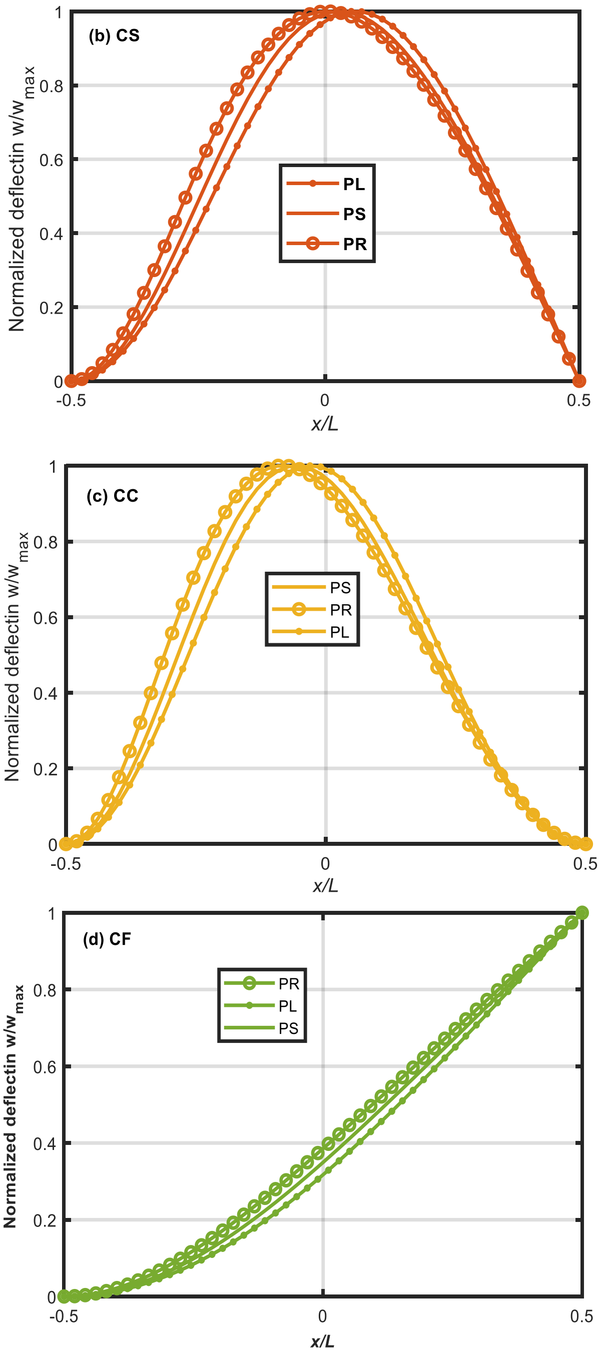

Fig. 9 Influence of axial parabolic load distributions: N_{PR} ,N_{PL} , and N_{PS} , on buckling mode shapes of FGM beams for different boundary conditions

5. Conclusions

Through this manuscript, buckling stability and mod-shapes of symmetric and sigmoid FG beams are investigated under distributed axial loads for different boundary conditions. The higher order shear deformation beam theory is exploited to include the shear effect, extension bending, and rigidity of the beam structure. Numerical DQM with the Chebyshev–Gauss–Lobatto distribution is employed to solve the equilibrium equations and evaluate critical buckling loads and associated mode-shapes. The finding of the current analysis can be summarized as:

- The effect of gradation index on the buckling load is dependent mainly on the gradation function type.
- In cases of symmetric power MCM and Sigmoid functions, critical buckling loads are decreased in exponential form as the gradation index increased and reached to steady state at $30 < k$.
- However, the inverse effect of gradation index on the critical buckling load has been observed in case of symmetric CMC functions distribution.
- It is noticed that at $k = 0$, the higher buckling load is observed for CMC gradation function and lower buckling load is noticed for MCM gradation type.
- For higher value of gradation index at $5 < k$, the higher buckling load is observed for MCM gradation function and lower buckling load is noticed for CMC gradation type.
- The loading type has effect on the critical buckling loads. The highest buckling load is observed in case of $\boldsymbol{N_{PR}}$ and the smallest buckling load is noticed in case of $\boldsymbol{N_{PL}}$ for all boundary conditions
- The type of axial load and boundary conditions have notable effects on the buckling mode shapes of FG beams.

References

Abdelrahman, A.A., Eltaher, M.A., Kabeel, A.M., Abdraboh, A. M. and Hendi, A.A. (2019), "Free and forced analysis of perforated beams", *Steel Compos. Struct.*, **31**(5), 489-502. https://doi.org/10.12989/scs.2019.31.5.489.

Abdulrazzaq, M.A., Fenjan, R.M., Ahmed, R.A. and Faleh, N.M. (2020), "Thermal buckling of nonlocal clamped exponentially graded plate according to a secant function based refined theory", *Steel Compos. Struct.*, **35**(1), 147-157. https://doi.org/10.12989/scs.2020.35.1.147.

Akbaş, Ş.D. (2018), "Geometrically nonlinear analysis of functionally graded porous beams", *Wind Struct.*, **27**(1), 59-70. https://doi.org/10.12989/was.2018.27.1.059.

Almitani, K.H., Abdelrahman, A.A. and Eltaher, M.A. (2019), "On forced and free vibrations of cutout squared beams", *Steel Compos. Struct.*, **32**(5), 643-655. https://doi.org/10.12989/scs.2019.32.5.643.

Almitani, K.H., Abdelrahman, A.A. and Eltaher, M.A. (2020), "Stability of perforated nanobeams incorporating surface energy effects", *Steel Compos. Struct.*, **35**(4), 555-566. https://doi.org/10.12989/scs.2020.35.4.555.

Aminbaghai, M., Murin, J. and Kutiš, V. (2012), "Modal analysis of the FGM-beams with continuous transversal symmetric and longitudinal variation of material properties with effect of large axial force", *Eng. Struct.*, **34**, 314-329. https://doi.org/10.1016/j.engstruct.2011.09.022.

Aminbaghai, M., Murin, J., Kutiš, V., Hrabovsky, J., Kostolani, M. and Mang, H.A. (2019), "Torsional warping elastostatic analysis of FGM beams with longitudinally varying material properties", *Eng. Struct.*, **200**, 109694. https://doi.org/10.1016/j.engstruct.2019.109694

Ansari, R., Hassani, R. and Torabi, J. (2019), "Mixed-type formulation of higher-order shear deformation theory for vibration and buckling analysis of FG-GPLRC plates using VDQFEM", *Compos. Struct.*, 111738. https://doi.org/10.1016/j.compstruct.2019.111738.

Alshorbagy, A.E., Eltaher, M.A. and Mahmoud, F.F. (2011), "Free vibration characteristics of a functionally graded beam by finite element method", *Appl. Math. Model.*, **35**(1), 412-425. https://doi.org/10.1016/j.apm.2010.07.006.

Arioui, O., Belakhdar, K., Kaci, A. and Tounsi, A. (2018), "Thermal buckling of FGM beams having parabolic thickness variation and temperature dependent materials", *Steel Compos. Struct.*, **27**(6), 777-788. https://doi.org/10.12989/scs.2018.27.6.777.

Avcar, M. (2019), "Free vibration of imperfect sigmoid and power law functionally graded beams", *Steel Compos. Struct.*, **30**(6), 603-615. https://doi.org/10.12989/scs.2019.30.6.603.

Benoy, M.B. (1969), "An energy solution to the buckling of rectangular plates under non-uniform in-plane loading", *Aeronaut. J.*, **73**(707), 974-977. https://doi.org/10.1017/S0001924000051423.

Bert, C.W. and Devarakonda, K.K. (2003), "Buckling of rectangular plates subjected to nonlinearly distributed in-plane loading", *Int. J. Solids Struct.*, **40**(16), 4097-4106. https://doi.org/10.1016/S0020-7683(03)00205-1.

Duan, W.H. and Wang, C.M. (2008), "Exact solution for buckling of columns including self-weight", *J. Eng. Mech.*, **134**(1), 116-119. https://doi.org/10.1061/(ASCE)0733-9399(2008)134:1(116)

Eisenberger, M. (1991), "Buckling loads for variable cross-section members with variable axial forces", *Int. J. Solids Struct.*, **27**(2), 135-143. https://doi.org/10.1016/0020-7683(91)90224-4.

Eltaher, M.A., Emam, S.A. and Mahmoud, F.F. (2012), "Free vibration analysis of functionally graded size-dependent nanobeams", *Appl. Math. Comput.*, **218**(14), 7406-7420. https://doi.org/10.1016/j.amc.2011.12.090.

Eltaher, M.A., Alshorbagy, A.E. and Mahmoud, F.F. (2013a), "Determination of neutral axis position and its effect on natural frequencies of functionally graded macro/nanobeams", *Compos. Struct.*, **99**, 193-201. https://doi.org/10.1016/j.compstruct.2012.11.039.

Eltaher, M.A., Emam, S.A. and Mahmoud, F.F. (2013b), "Static and stability analysis of nonlocal functionally graded nanobeams", *Compos. Struct.*, **96**, 82-88, https://doi.org/10.1016/j.compstruct.2012.09.030.

Eltaher, M.A., Khairy, A., Sadoun, A.M. and Omar, F.A. (2014), "Static and buckling analysis of functionally graded Timoshenko nanobeams", *Appl. Math. Comput.*, **229**, 283-295. https://doi.org/10.1016/j.amc.2013.12.072.

Eltaher, M.A., Khater, M.E., Park, S., Abdel-Rahman, E. and Yavuz, M. (2016), "On the static stability of nonlocal nanobeams using higher-order beam theories", *Adv. Nano Res.*, **4(**1), 51-64. https://doi.org/10.12989/anr.2016.4.1.051.

Eltaher, M.A., Mohamed, N., Mohamed, S.A. and Seddek, L.F. (2019), "Periodic and nonperiodic modes of postbuckling and nonlinear vibration of beams attached to nonlinear foundations", *Appl. Math. Model.*, **75**, 414-445. https://doi.org/10.1016/j.apm.2019.05.026.

Eltaher, M.A., Mohamed, S.A. and Melaibari, A. (2020). Static stability of a unified composite beams under varying axial loads. *Thin-Wall. Struct.*, 147, 106488. https://doi.org/10.1016/j.tws.2019.106488.

Eltaher, M.A. and Mohamed, S.A. (2020), "Buckling and Stability Analysis of Sandwich Beams subjected to Varying Axial Loads", *Steel Compos. Struct.*, **34**(2), 241-260, https://doi.org/10.12989/scs.2020.34.2.241.

Emam, S. and Eltaher, M.A. (2016), "Buckling and postbuckling of composite beams in hygrothermal environments", *Compos. Struct.*, **152**, 665-675. https://doi.org/10.1016/j.compstruct.2016.05.029.

Emam, S.A., Eltaher, M.A., Khater, M.E. and Abdalla, W.S. (2018), "Postbuckling and free vibration of multilayer imperfect nanobeams under a pre-stress load", *Appl. Sci.*, **8**(11), 2238. https://doi.org/10.3390/app8112238.

Farajpour, A., Shahidi, A.R., Mohammadi, M. and Mahzoon, M. (2012), "Buckling of orthotropic micro/nanoscale plates under linearly varying in-plane load via nonlocal continuum mechanics", *Compos. Struct.*, **94**(5), 1605-1615. https://doi.org/10.1016/j.compstruct.2011.12.032.

Hamed, M.A., Eltaher, M.A., Sadoun, A.M. and Almitani, K.H. (2016), "Free vibration of symmetric and sigmoid functionally graded nanobeams", *Appl. Phys. A*, **122**(9), 829. https://doi.org/10.1007/s00339-016-0324-0.

Hamed, M.A., Sadoun, A.M. and Eltaher, M.A. (2019), "Effects of porosity models on static behavior of size dependent functionally graded beam", *Struct. Eng. Mech.*, **71**(1), 89-98. https://doi.org/10.12989/sem.2019.71.1.089.

Hamed M.A., Mohamed, S.A. and Eltaher, M.A. (2020a), "Buckling analysis of sandwich beam rested on elastic foundation and subjected to varying axial in-Plane Loads", *Steel Compos. Struct.*, **34**(1), 75-89. https://doi.org/10.12989/scs.2020.34.1.075.

Hamed M.A., Abu-bakr, R.M., Mohamed, S.A. and Eltaher, M.A. (2020b), "influence of Axial Load Function and Optimization on Static Stability of Sandwich Functionally Graded Beams with Porous Core", *Eng. with Comput.*, 1-14. https://doi.org/10.1007/s00366-020-01023-w.

Hamed M.A, Mohamed, N.A. and Eltaher, M.A. (2020c), "Stability buckling and bending of nanobeams including cutouts", *Eng. with Comput.*, 1-14. https://doi.org/10.1007/s00366-020-01063-2.

Kahya, V. and Turan, M. (2017), "Finite element model for vibration and buckling of functionally graded beams based on the first-order shear deformation theory", *Compos. Part B: Eng.*, **109**, 108-115. https://doi.org/10.1016/j.compositesb.2016.10.039.

Kang, J.H. and Leissa, A.W. (2005), "Exact solutions for the buckling of rectangular plates having linearly varying in-plane loading on two opposite simply supported edges", *International J. Solids Struct.*, **42**(14), 4220-4238. https://doi.org/10.1016/j.ijsolstr.2004.12.011.

Karamanli, A. and Aydogdu, M. (2019a), "Buckling of laminated composite and sandwich beams due to axially varying in-plane loads", *Compos. Struct.*, **210**, 391-408. https://doi.org/10.1016/j.compstruct.2018.11.067.

Karamanli, A. and Aydogdu, M. (2019b), "Free vibration and buckling analysis of laminated composites and sandwich microbeams using a transverse shear-normal deformable beam theory", *J. Vib. Control*, 1077546319878538. https://doi.org/10.1177/1077546319878538.

Karami, B., Shahsavari, D., Nazemosadat, S.M.R., Li, L. and Ebrahimi, A. (2018), "Thermal buckling of smart porous functionally graded nanobeam rested on Kerr foundation", *Steel Compos. Struct.*, **29**(3), 349-362. https://doi.org/10.12989/scs.2018.29.3.349.

Khorshidi, M.A., Shariati, M. and Emam, S.A. (2016), "Postbuckling of functionally graded nanobeams based on modified couple stress theory under general beam theory", *Int. J. Mech. Sci.*, **110**, 160-169. https://doi.org/10.1016/j.ijmecsci.2016.03.006 .

Kim, H.J., Yoon, K. and Lee, P.S. (2020), "Continuum mechanics based beam elements for linear and nonlinear analyses of multi-layered composite beams with interlayer slips", *Compos. Struct.*, 111740. https://doi.org/10.1016/j.compstruct.2019.111740.

Lou, J., He, L., Wu, H. and Du, J. (2016), "Pre-buckling and buckling analyses of functionally graded microshells under axial and radial loads based on the modified couple stress theory", *Compos. Struct.*, **142**, 226-237. https://doi.org/10.1016/j.compstruct.2016.01.083.

Mijušković, O., Ćorić, B. and Šćepanović, B. (2014), "Exact stress functions implementation in stability analysis of plates with different boundary conditions under uniaxial and biaxial compression", *Thin-Wall. Struct.*, **80**, 192-206. https://doi.org/10.1016/j.tws.2014.03.006.

Mohamed, N., Eltaher, M.A., Mohamed, S.A. and Seddek, L.F. (2018), "Numerical analysis of nonlinear free and forced vibrations of buckled curved beams resting on nonlinear elastic foundations", *Int. J. Nonlinear Mech.*, **101**, 157-173. https://doi.org/10.1016/j.ijnonlinmec.2018.02.014.

Mohamed, N., Eltaher, M.A., Mohamed, S.A. and Seddek, L.F. (2019), "Energy equivalent model in analysis of postbuckling of imperfect carbon nanotubes resting on nonlinear elastic foundation", *Struct. Eng. Mech.*, **70**(6), 737-750. https://doi.org/10.12989/sem.2019.70.6.737.

Mohamed, N., Mohamed, S.A. and Eltaher, M.A. (2020), "Buckling and post-buckling behaviors of higher order carbon nanotubes using energy-equivalent model", *Eng. with Comput.*, 1-14. https://doi.org/10.1007/s00366-020-00976-2.

Mohammadimehr, M., Mohammadi-Dehabadi, A.A., Akhavan Alavi, S.M., Alambeigi, K., Bamdad, M., Yazdani, R. and Hanifehlou, S. (2018), "Bending, buckling, and free vibration analyses of carbon nanotube reinforced composite beams and experimental tensile test to obtain the mechanical properties of nanocomposite", *Steel Compos. Struct.*, **29**(3), 405-422. https://doi.org/10.12989/scs.2018.29.3.405.

Murín, J., Aminbaghai, M., Hrabovský, J., Kutiš, V., Paulech, J., and Kugler, S. (2016), "Elastostatic and modal and buckling analysis of spatial FGM beam structures", *Proceedings of the VII European Concress on Computational Methods in Applied Sciences and Engineering* (ECCOMAS Congress 2016)", National Technical University of Athens (NTUA), 2016, Paper-Nr. 4649, 28 S.

Osmani, A. and Meftah, S.A. (2018), "Lateral buckling of tapered thin walled bi-symmetric beams under combined axial and bending loads with shear deformations allowed", *Eng. Struct.*, **165**, 76-87. https://doi.org/10.1016/j.engstruct.2018.03.009.

Panda, S.K. and Ramachandra, L.S. (2010), "Buckling of rectangular plates with various boundary conditions loaded by non-uniform inplane loads", *Int. J. Mech. Sci.*, **52**(6), 819-828. https://doi.org/10.1016/j.ijmecsci.2010.01.009.

Polit, O., Merzouki, T. and Ganapathi, M. (2018), "Elastic stability of curved nanobeam based on higher-order shear deformation theory and nonlocal analysis by finite element approach", *Finite Elem. Anal. Des.*, **146**, 1-15. https://doi.org/10.1016/j.finel.2018.04.002.

Rahmani, O., Hosseini, S.A.H. and Parhizkari, M. (2017), "Buckling of double functionally-graded nanobeam system under axial load based on nonlocal theory: an analytical approach", *Microsystem Technologies*, **23**(7), 2739-2751. DOI 10.1007/s00542-016-3127-5.

Ravindran, A. and Bhaskar, K. (2019), "Three-dimensional analysis of composite FGM rectangular plates with in-plane heterogeneity", *Int. J. Mech. Sci.*, **160**, 386-396. https://doi.org/10.1016/j.ijmecsci.2019.07.004.

Reddy, J.N. (1984), "A simple higher-order theory for laminated composite plates", *J. Appl. Mech.*, **51**(4), 745-752. https://doi.org/10.1115/1.3167719

Robinson, M.T.A. and Adali, S. (2016), "Variational solution for buckling of nonlocal carbon nanotubes under uniformly and triangularly distributed axial loads", *Compos. Struct.*, **156**, 101-107. https://doi.org/10.1016/j.compstruct.2016.01.026.

Sedighi, H.M., Keivani, M. and Abadyan, M. (2015a), Modified continuum model for stability analysis of asymmetric FGM double-sided NEMS: corrections due to finite conductivity, surface energy and nonlocal effect", *Compos. Part B: Eng*., **83**, 117-133. https://doi.org/10.1016/j.compositesb.2015.08.029.

Sedighi, H.M., Daneshmand, F. and Abadyan, M. (2015b), "Modified model for instability analysis of symmetric FGM double-sided nano-bridge: corrections due to surface layer, finite conductivity and size effect", *Compos. Struct.*, **132**, 545-557. https://doi.org/10.1016/j.compstruct.2015.05.076.

She, G.L., Yuan, F.G. and Ren, Y.R. (2017), "Thermal buckling and post-buckling analysis of functionally graded beams based on a general higher-order shear deformation theory", *Appl. Math. Model.*, **47**, 340-357. https://doi.org/10.1016/j.apm.2017.03.014.

Shu, C. (2012). Differential quadrature and its application in engineering. Springer Science & Business Media.

Şimşek, M. and Reddy, J.N. (2013), "A unified higher order beam theory for buckling of a functionally graded microbeam embedded in elastic medium using modified couple stress theory", *Compos. Struct.*, **101**, 47-58. https://doi.org/10.1016/j.compstruct.2013.01.017

Singh, S.J. and Harsha, S.P. (2019), "Buckling analysis of FGM plates under uniform, linear and non-linear in-plane loading", *J. Mech. Sci. Technol.*, **33**(4), 1761-1767. DOI 10.1007/s12206-019-0328-8

Wang, J.T.S., Biggerst, S.B. and Dickson, J.N. (1984), "Buckling of composite plates with a free edge in edgewise bending and compression", *AIAA J.*, **22**(3), 394-398. https://doi.org/10.2514/3.48460.

CC